Structure, Vol. 11, 1151–1161, September, 2003, ©2003 Elsevier Science Ltd. All rights reserved. DOI 10.1016/S0969-2126(03)00187-4

Structural, Energetic, and Functional Analysis of a Protein-Protein Interface at Distinct Stages of Affinity Maturation

Eric J. Sundberg,[1,*] Peter S. Andersen,[2] Patrick M. Schlievert,[3] Klaus Karjalainen,[4] and Roy A. Mariuzza[1]

[1]Center for Advanced Research in Biotechnology
W.M. Keck Laboratory for Structural Biology
University of Maryland Biotechnology Institute
9600 Gudelsky Drive
Rockville, Maryland 20850

[2]Symphogen A/S
Elektrovej, Building 375
DK-2800 Lyngby
Denmark

[3]Department of Microbiology
University of Minnesota Medical School
Minneapolis, Minnesota 55455

[4]Istituto di Ricerca in Biomedicina
Via Vincenzo Vela 6
CH-6500 Bellinzona
Switzerland

Summary

Due to a paucity of studies that synthesize structural, energetic, and functional analyses of a series of protein complexes representing distinct stages in an affinity maturation pathway, the biophysical basis for the molecular evolution of protein-protein interactions is poorly understood. Here, we combine crystal structures and binding-free energies of a series of variant superantigen (SAG)-major histocompatibility complex (MHC) class II complexes exhibiting increasingly higher affinity to reveal that this affinity maturation pathway is controlled largely by two biophysical factors: shape complementarity and buried hydrophobic surface. These factors, however, do not contribute equivalently to the affinity maturation of the interface, as the former dominates the early steps of the maturation process while the latter is responsible for improved binding in later steps. Functional assays reveal how affinity maturation of the SAG-MHC interface corresponds to T cell activation by SAGs.

Introduction

The ability of proteins to associate in a specific and stable manner is a hallmark of myriad cellular processes—from signal transduction to cytoskeletal remodeling, from immune signaling to vesicle transport. The biophysical factors that can influence molecular recognition between proteins are also highly diverse, including van der Waals interactions, hydrogen bonding, hydrophobic packing, shape and charge complementarity, allostery, cooperativity, and plasticity (Bogan and Thorn, 1998; Conte et al., 1999; DeLano, 2002; Ma et al., 2001; Sheinerman et al., 2000; Sundberg and Mariuzza, 2000; Wodak and Janin, 2002). With such disparate lists of required functions and contributing factors, it is not surprising that protein-protein interactions are exceedingly complex and incompletely understood.

Biophysical characterization, including structural and energetic analysis, of model protein-protein interaction systems perturbed in a controlled manner have yielded numerous meaningful quantitative correlations between refined structures and measured binding energies (Bogan and Thorn, 1998; Brooijmans et al., 2002; Hilser et al., 1996; Kuntz et al., 1999; Lavigne et al., 2000; Luque and Freire, 2002; Wodak and Janin, 2002). These correlations are crucial to the design of general algorithms needed to predict the specificities and energies of protein-protein interactions from protein structures alone, predictive tools that are becoming increasingly important in the postgenomic era of biochemical research. We have previously sought to establish such correlations through the combination of site-directed mutagenesis of single residues within a protein interface coupled with X-ray crystallographic determination of the mutant complex structures and calorimetric analysis of their binding energetics (Sundberg and Mariuzza, 2002). For example, by altering an energetically important interface residue within the antigen binding site of an antibody, this strategy has allowed us to calculate the magnitude of the hydrophobic effect in a protein-protein interface (Sundberg et al., 2000).

While highly controlled, these single point mutagenesis experiments are aimed at quantifying the effect of a single biophysical factor. The affinity maturation process, by which proteins have evolved over time to bind one another with improved affinity and specificity, however, simultaneously calls upon the entire arsenal of biophysical factors that govern molecular recognition. Structural and energetic analysis of a protein complex at discreet stages of affinity maturation may then provide insight into the relative utilization and energetic magnitudes of various biophysical factors in the maturation process and result in more accurate and generally applicable structure binding correlations than analysis of a series of single site mutants.

Since associating proteins along the affinity maturation pathway are relegated to the evolutionary dustbin as the more mature complexes appear, it is not possible to recover genetic fragments encoding proteins corresponding to distinct affinity maturation steps. In vitro-directed evolution techniques, such as phage display mutagenesis (Lowman, 1997), can be used, however, to mimic in vivo affinity maturation, especially with relatively low-affinity protein complexes. This can result in a series of variants that individually represent distinct stages of affinity maturation and together define the affinity maturation pathway. A further benefit of directed evolution is the ability to restrict evolutionary pressure to a relatively small portion of the molecular interface, thereby simplifying the structural and energetic analysis and allowing the derivation of meaningful correlations. Directed evolution techniques may be particularly pow-

*Correspondence: sundberg@umbi.umd.edu

erful in deciphering the affinity maturation process as they allow for simultaneous and synergistic changes to multiple interface residues and the possibility of producing binding solutions with fundamentally different structural properties as compared to the original interaction (Dwyer et al., 2001), experimental options not available to site-directed mutagenesis approaches.

To better define the structural basis for protein-protein affinity maturation, we have combined phage display mutagenesis, X-ray crystallographic structure determination, binding analysis, and functional characterization of a series of variants of the superantigen (SAG) staphylococcal enterotoxin C3 (SEC3) in complex with the class II major histocompatibility complex (MHC) molecule HLA-DR1. The SEC3/HLA-DR1 complexes analyzed represent discreet stages of affinity maturation in a process encompassing a nearly 60-fold increase in affinity. Analogously, we have analyzed the interaction between HLA-DR1 and SEB, which is highly similar to SEC3 and represents another intermediate along the SEC3 affinity maturation pathway. We find that affinity maturation of the SAG-MHC interface is dependent primarily on improved shape complementarity and increase burial of hydrophobic surface, that these biophysical factors affect early and late steps in the maturation pathway differentially, and that the extent of affinity maturation determines the level to which this interface controls SAG biological activity within the functionally relevant supramolecular complex.

Results and Discussion

Overview of the Wild-Type and Mutant SEC3/HLA-DR1 Crystal Structures

We have solved crystal structures of the MHC class II molecule HLA-DR1 with wild-type SEC3 (SEC3-wt) and two phage display variants thereof (SEC3-3B1 and SEC3-3B2) that vary in the hydrophobic ridge residues 43–47 (Andersen et al., 1999). Data collection and refinement statistics are shown in Table 1, and σ_A-weighted omit electron density maps for the SEC3 variant residues 43–47 are shown in Figure 1. Structural differences between the three complexes are confined to those residues varied by phage display plus the neighboring invariant residue Asn42, whose atomic position varies slightly between the SEC3 molecules. The root mean square deviation for all C^α atoms outside of this region for the three SEC3/HLA-DR1 crystal structures is 0.3 Å. These structures represent discreet snapshots of an affinity maturation process that spans a nearly 60-fold difference in affinity. The respective variant sequences and binding affinities for SEC3-wt, SEC3-3B1, SEC3-3B2, as well as the highly homologous SAG SEB are shown in Table 2.

Within the variable interfaces of the SEC3-wt, SEC3-3B1, and SEC3-3B2/HLA-DR1 complexes there are no significant differences in the overall number or type of intermolecular contacts (Figure 2). Additionally, two of the hydrogen bonds, those formed between the terminal atoms of Tyrα13 and Lysα67 and main chain atoms of the SEC3 molecules, are conserved in all three SEC3/HLA-DR1 complexes. It is therefore unlikely that the significant affinity differences in the wild-type and variant SEC3 interactions with HLA-DR1 are attributable to relative distinctions in intermolecular contacts. Substitution of residues Leu45 and His47 in SEC3-wt with the bulkier aromatic amino acids Phe and Trp in both SEC3-3B1 and SEC3-3B2, however, does result in a relative increase in the number of van der Waals interactions between these particular side chains and HLA-DR1. Furthermore, these hydrophobic side chains extend further into the concave HLA-DR1 surface. The relative impact of these contacts can be understood most clearly through an analysis of the changes in accessible surface area buried upon complex formation as well as the shape and charge complementarity of the resulting interfaces.

Interactions of the variable regions of SEC3-wt, SEC3-3B1, and SEC3-3B2 (residues 43–47) plus Asn42 with the HLA-DR1 α subunit result in total buried surface areas of 632, 688, and 674 Å^2, respectively (Table 2). These values for changes in accessible surface area (ΔASA) upon complex formation are more meaningful, however, when deconstructed on the basis of individual

Table 1. Data Collection and Refinement Statistics for Wild-Type and Mutant SEC3-DR1 Complexes

	SEC3-wt	SEC3-3B1	SEC3-3B2
Data Collection			
Space group	*R3*	*R3*	*R3*
Cell dimensions			
a (Å)	171.695	170.395	171.753
c (Å)	120.796	120.812	120.489
Temperature (K)	100	100	100
Resolution limit (Å)	2.7	2.6	2.3
Mosaicity (°)	0.8	0.6	0.3
Unique reflections	34,242	40,189	58,678
Total observations	134,545	228,880	172,353
Completeness (%)	94.1 (94.9)[a]	99.8 (100)	99.6 (99.7)
Mean I/σ (I)	15.4 (3.0)	21.3 (2.6)	14.8 (2.8)
R_{sym} (%)[b]	8.5 (31.6)	7.1 (49.5)	6.7 (42.1)
Refinement			
R_{free}[c]	22.8 (30.5)	23.2 (27.4)	23.7 (28.8)
R_{cryst}	19.2 (25.3)	19.5 (24.5)	20.0 (24.5)
Protein			
Residues	612	612	612
Average B (Å^2)	40.3	44.2	35.7
Water			
Molecules	139	141	178
Average B (Å^2)	32.9	36.4	33.3
RMS deviations from ideality			
Bonds (Å)	0.008	0.008	0.007
Angles (°)	1.361	1.373	1.326
Ramachandran plot statistics			
Core (%)	85.6	86.2	89.0
Allowed (%)	13.1	12.4	10.3
Generous (%)	1.3	1.3	0.6
Disallowed (%)	0.0	0.2	0.2

[a] Values in parentheses correspond to the highest resolution shell: wild-type (2.80–2.70 Å); 3B1 (2.69-2.60 Å); 3B2 (2.38–2.30 Å).
[b] $R_{sym} = \Sigma|I - \langle I\rangle|/\Sigma\langle I\rangle$, where I is the observed intensity and $\langle I\rangle$ is the average intensity of multiple observations of symmetry-related reflections.
[c] A portion of the overall reflections was set aside for R_{free} calculations: wild-type (1473, 4.1%); 3B1 (1669, 4.2%); 3B2 (2548, 4.3%).

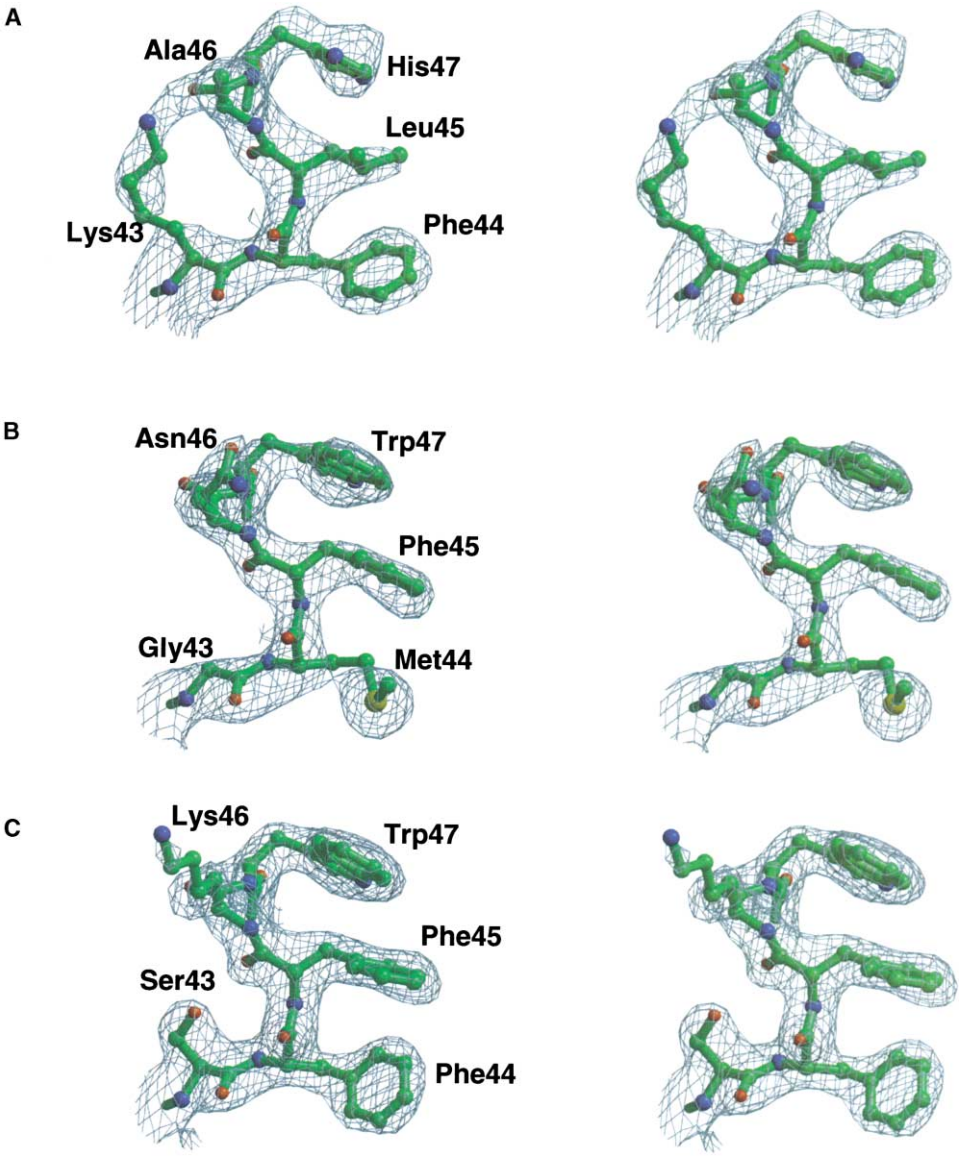

Figure 1. Structural Validation of the Wild-Type and Mutant SEC3-DR1 Complexes

Stereodiagrams of composite annealed omit electron density maps in the variant region (residues 43–47) of (A) SEC3-wt, (B) SEC3-3B1, and (C) SEC3-3B2. All electron density maps are contoured at 1.4σ. Figure produced using Bobscript (Esnouf, 1997) and Raster3D (Merritt and Bacon, 1997).

contributing residues and polarity. While there is no apparent correlation between ΔASA_{polar} values and binding affinities of the SEC3/HLA-DR1 complexes, discrepancies in ΔASA_{apolar} between the three complexes can, in part, explain these affinity differences. As affinity increases, so too does the total ΔASA_{apolar} from 383 to 398 to 425 Å^2 in the SEC3-wt, SEC3-3B1, and SEC3-3B2/HLA-DR1 complexes, respectively. Both SEC3-3B1 and SEC3-3B2 contain mutations of residues Leu45 and His47 to Phe45 and Trp47, respectively. As mentioned above, these mutations result in an increase in the number of van der Waals contacts formed between their side chains and residues Metα36, Alaα37, Leuα60, and Ileα63 of HLA-DR1 (Figure 2). There are likewise increases of approximately 10 and 20 Å^2 in ΔASA_{apolar} buried by residues 45 and 47, respectively, when the SEC3-wt/HLA-DR1 complex is compared to those formed between SEC3-3B1 and SEC3-3B2 and HLA-DR1. Residue 46 may also play an important role in the affinity differences of the SEC3/HLA-DR1 complexes. Because the Ala46 side chain in SEC3-wt contributes no intermolecular contacts to the complex and the SEC3-3B1 Asn46 side chain forms a hydrogen bond with the main chain of HLA-DR1 Aspα17 (Figures 2A and 2B), the ΔASA_{apolar} of the residues at position 46 of SEC3-wt and SEC3-3B1 are nearly identical when bound by HLA-DR1. Conversely, the long, aliphatic side chain of SEC3-3B2 Lys46, aligned along the HLA-DR1 surface, contributes

Table 2. Structural Characteristics of Superantigens Complexed with HLA-DR1

	SEC3-wt					SEC3-3B1					SEC3-3B2					SEB[a]				
Hydrophobic ridge	43	44	45	46	47	43	44	45	46	47	43	44	45	46	47	43	44	45	46	47
Amino acid sequence	K	F	L	A	H	G	M	F	N	W	S	F	F	K	W	Q	F	L	Y	F
K_D (μM)	270					14					4.6					54				
ΔG_b (kcal mol^{-1})[b]	−4.86					−6.62					−7.28					−5.82				
ΔASA (Å^2)[c]	Polar	Apolar	Aggregate			Polar	Apolar	Aggregate			Polar	Apolar	Aggregate			Polar	Apolar	Aggregate		
Superantigen	89	249	338			120	248	368			84	277	361			69	264	333		
HLA-DR1	160	134	294			170	150	320			165	148	313			127	141	268		
Total	249	383	632			290	398	688			249	425	674			196	405	601		
S_c[d]	0.710					0.837					0.817					0.758				

[a] Analysis of SEB/HLA-DR1 complex using PDB accession code 1SEB (Jardetzky et al., 1994).
[b] Calculated using $\Delta G_b = -RT\ln(K_D^{-1})$, where R is the universal gas constant (-1.9867 cal mol^{-1} K^{-1}), and T is temperature (298 K).
[c] ΔASA values calculated using the program AREAIMOL from the CCP4 Suite (CCP4, 1994) and a probe radius of 1.4 Å.
[d] S_c values calculated for the interface formed between the superantigen hydrophobic ridge sequence (residues 43–47) plus residue 42 and HLA-DR1.

additional van der Waals interactions (Figure 2C) with a relative increase in ΔASA_{apolar} of approximately 20 Å^2.

An important factor in regulating the affinity and specificity of a protein-protein interaction is the degree of complementarity, in terms of both shape and charge, in the apposing molecular surfaces of the interface. Shape complementarity is quantifiable using the S_c coefficient (Lawrence and Colman, 1993), which ranges from 0 (topologically uncorrelated) to 1 (perfect geometrical fit). S_c values for the interfaces formed by the variant SEC3 residues 43–47 plus Asn42 with the α subunit of HLA-DR1 are 0.710, 0.837, and 0.817 for the SEC3-wt, SEC3-3B1, and SEC3-3B2/HLA-DR1 complexes, respectively (Table 2). These shape complementarities can be mapped to the SEC3 molecular surfaces, providing a more information-dense S_c analysis (Figures 3A–3C). The most striking feature of the shape complementarity character of these interfaces is the marked increase in S_c value along the raised hydrophobic ridge in SEC3-3B1 and SEC3-3B2 relative to SEC3-wt (represented by a darkening of the blue color along the SEC3 hydrophobic ridge molecular surfaces, especially residues 44, 45, and 47). While there exist fewer topologically uncorrelated regions in the SEC3-wt/HLA-DR1 interface (note the diffuse blue color throughout the SEC3-wt molecular surface in Figure 3A), a concentration of shape complementarity along the hydrophobic ridge in the SEC3-3B1 and SEC3-3B2/HLA-DR1 interfaces (Figures 3B and 3C) toward local perfect geometrical fit significantly increases the global shape complementarity (dark blue), notwithstanding the presence of more numerous discreet regions of poor complementarity (white). One other important aspect of these relative shape complementarities is the interface dependent on the side chain of SEC3-3B2 residue Lys46 (Figure 3C), which contributes 47 Å^2 to ΔASA_{apolar}. Notably, much of this surface is colored white, indicating very low shape complementarity.

A depiction of charge complementarity (Figures 3D–3F) provides a visualization of the increasingly apolar character of the hydrophobic ridge in both SEC3-3B1 and SEC3-3B2. It also shows that the interface extension in the SEC3-3B2/HLA-DR1 complex contributed by Lys46 (Figure 3F) is almost entirely hydrophobic, as the amino group of the Lys46 side chain is largely outside of the molecular interface (the boundaries of which are defined by the black line).

Structural Basis of Affinity Maturation in a Protein-Protein Interface

Examining the structural and energetic characteristics of a protein-protein interaction at distinct stages of affinity maturation can provide a biophysical understanding of molecular evolution. By merging X-ray crystallographic analysis with measured affinities, we have identified two biochemical factors that appear to drive the affinity maturation process in the remodeling of the interface formed between SEC3 and HLA-DR1: augmentation of ΔASA_{apolar} and improvement in shape complementarity.

Previously, we determined an experimental value of -21 cal mol^{-1} Å^{-2} for the hydrophobic binding free energy in an antibody-antigen protein-protein interac-

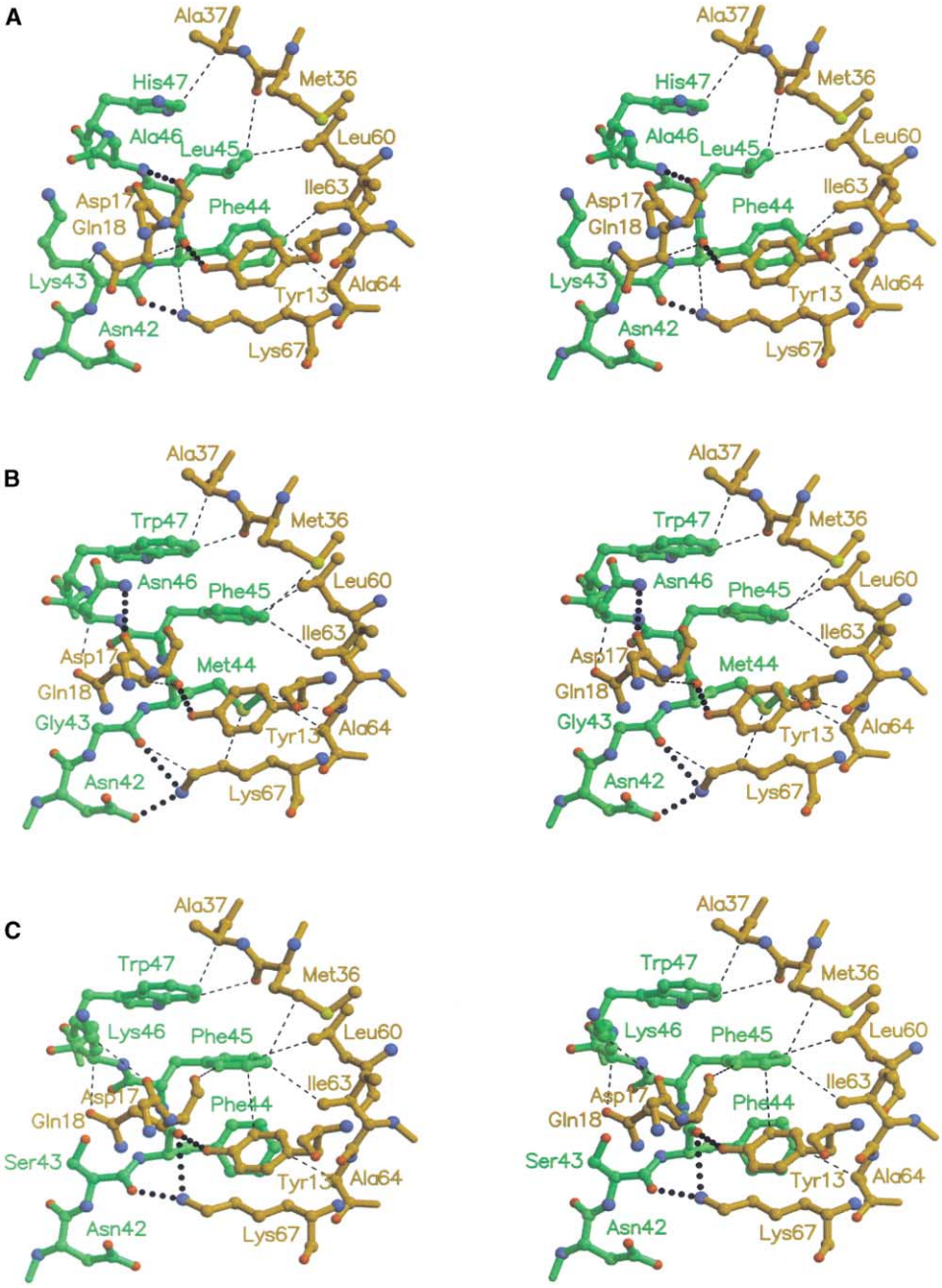

Figure 2. Intermolecular Contacts in the Wild-Type and Mutant SEC3-DR1 Complexes

Stereodiagrams depicting the intermolecular contacts in the (A) SEC3-wt, (B) SEC3-3B1, and (C) SEC3-3B2 complexes with HLA-DR1. In all panels, SEC3 residues are shown in green; DR1 α subunit residues in orange. Hydrogen-bonding interactions are represented by dotted lines; van der Waals interactions by dashed lines. Maximum contact distances (in Å) are as follows: C-C, 4.1; C-N, 3.8; C-O, 3.7; O-O, 3.3; O-N, 3.4; N-N, 3.4. Figure produced using Molscript (Kraulis, 1991) and Raster3D (Merritt and Bacon, 1997).

tion (Sundberg et al., 2000). Applying this estimation of the hydrophobic effect to the SEC3/HLA-DR1 system shows that affinity maturation can be explained solely by increases in ΔASA_{apolar} within the molecular interfaces for the latter step of the SEC3 affinity maturation pathway, namely the maturation step between SEC3-3B1 and SEC3-3B2. The difference in the free energy of binding between SEC3-3B2 and SEC3-3B1 interactions with HLA-DR1 [Table 2; $\Delta G_{b(SEC3\text{-}3B2/HLA\text{-}DR1)} - \Delta G_{b(SEC3\text{-}3B1/HLA\text{-}DR1)} = \Delta\Delta G_{b(3B2\text{-}3B1)}$] is -0.66 kcal mol^{-1}. The difference in ΔASA_{apolar} [Table 2; $\Delta ASA_{apolar(SEC3\text{-}3B2/HLA\text{-}DR1)} - \Delta ASA_{apolar(SEC3\text{-}3B1/HLA\text{-}DR1)} = \Delta\Delta ASA_{apolar(3B2\text{-}3B1)}$] is 27 Å^2 from which a predicted difference in the free energy of binding [$\Delta\Delta G_{predicted(3B2\text{-}3B1)} = (-21$ cal mol^{-1} Å^{-2})$\Delta\Delta ASA_{apolar(3B2\text{-}3B1)}$] is calculated to

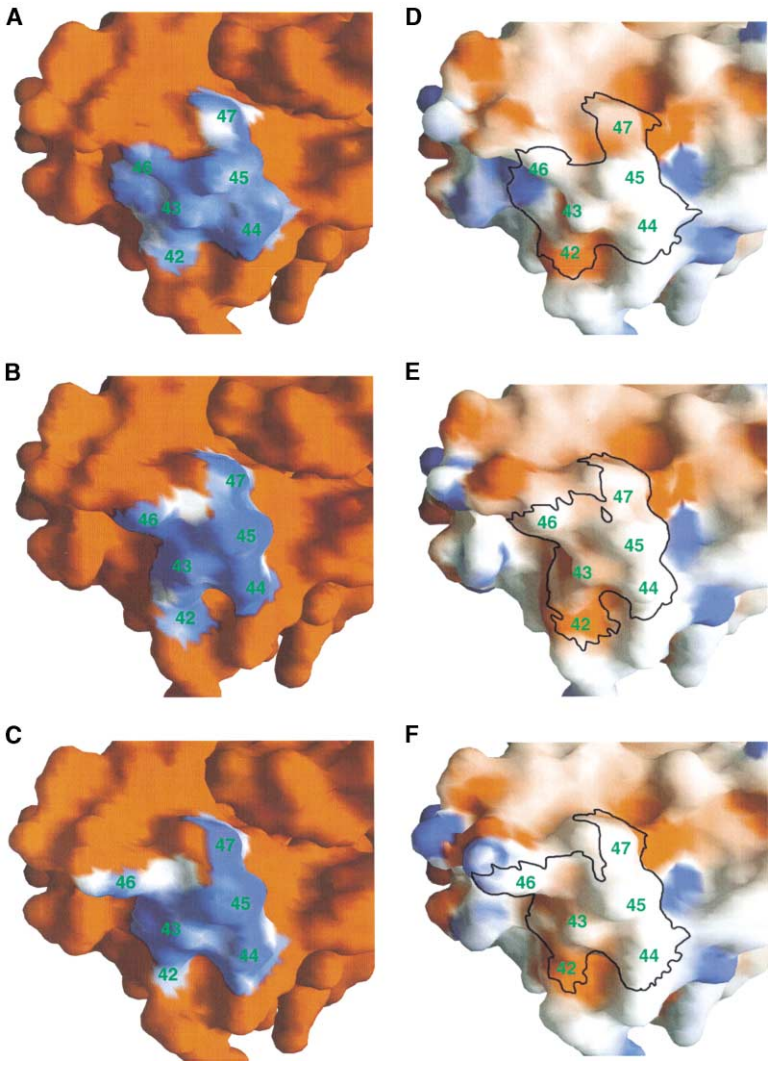

Figure 3. Shape Complementarity and Electrostatic Properties of the Wild-Type and Mutant SEC3 Variant Regions

The molecular surface of the variant regions (residues 43–47) plus residue Asn42 of (A) SEC3-wt, (B) SEC3-3B1, and (C) SEC3-3B2 in contact with the HLA-DR1 α subunit, in which shape complementarity (Lawrence and Colman, 1993) values are shown scaled from 0 (white, no complementarity) to 1 (dark blue, perfect complementarity). The red surface lies outside of this interface region. SEC3 molecular surfaces, in which electronegative (red, -10 kT), electropositive (blue, $+10$ kT), and apolar (white) surfaces are shown for (D) SEC3-wt, (E) SEC3-3B1, and (F) SEC3-3B2. The black line surrounds the interface region between the variant regions plus residue Asn42 of the SEC3 molecules and the HLA-DR1 α subunit as determined by shape complementarity analysis. SEC3 residue numbers are labeled in green. Figure produced using Grasp (Nicholls et al., 1991).

be -0.57 kcal mol^{-1}. Thus, $\Delta\Delta ASA_{apolar(3B2\text{-}3B1)}$ adequately describes affinity changes in the molecular evolution process associated with mutagenesis of SEC3-3B1 to SEC3-3B2.

Changes in ΔASA_{apolar} alone, however, are inadequate in describing affinity differences resulting from mutagenesis of SEC3-wt to either the intermediate affinity (SEC3-3B1) or high-affinity (SEC3-3B2) variants. On account of the differences in ΔASA_{apolar} between these complexes, where $\Delta\Delta ASA_{apolar(3B1\text{-}wt)}$ is 15 Å^2 and $\Delta\Delta ASA_{apolar(3B2\text{-}wt)}$ is 42 Å^2, and using the above estimate of the hydrophobic effect (Sundberg et al., 2000) to calculate predicted free energies of binding gives a $\Delta\Delta G_{predicted(3B1\text{-}wt)}$ of -0.32 kcal mol^{-1} and a $\Delta\Delta G_{predicted(3B2\text{-}wt)}$ of -0.88 kcal mol^{-1}. These predicted values are both significantly lower than the actual differences in the free energy of binding between the SEC3-wt/HLA-DR1 complex with the SEC3-3B1/HLA-DR1 and SEC3-3B2/HLA-DR1 complexes, where $\Delta\Delta G_{b(3B1\text{-}wt)}$ is -1.76 kcal mol^{-1} and $\Delta\Delta G_{b(3B2\text{-}wt)}$ is -2.42 kcal mol^{-1}, respectively.

One biophysical factor that varies among these complexes and may explain the measured affinity differences between the SEC3-wt/HLA-DR1 complex and HLA-DR1 complexes with both SEC3-3B1 and SEC3-3B2, is the degree of shape complementarity in the variant region of the interface. The S_c values for this region of the interface are 0.710, 0.837, and 0.817 for the SEC3-wt, SEC3-3B1, and SEC3-3B2/HLA-DR1 complexes, respectively (Table 2), indicating that augmentation of shape complementarity in a restricted region of the protein-protein interface can significantly affect overall binding affinity. It appears, though, that there may be an S_c value ceiling for this affinity maturation pathway. Oligomeric proteins and protease-protease inhibitor complexes, systems in which the affinity maturation process has perhaps been exhausted, commonly exhibit S_c values for the overall interface ranging from 0.70 to 0.76 (Jones and Thornton, 1996). Discreet regions within these interfaces certainly vary significantly in shape complementarity, much like the variant regions in the SEC3/HLA-DR1 complexes. The S_c values of the entire (variant plus nonvariant regions) SEC3/HLA-DR1 interfaces are 0.67, 0.73, and 0.70 for the SEC3-wt, SEC3-3B1, and SEC3-3B2/HLA-DR1 complexes, respectively.

Although it may prove merely coincidental, this overall interface S_c value threshold for improved binding via affinity maturation in the SEC3/HLA-DR1 complexes, 0.70, is equivalent to the lower limit for protein-protein interfaces which may have reached an evolutionary endpoint in terms of affinity maturation.

Thus, there appears to be a dual mechanism of affinity maturation at play in the directed evolution of SEC3 interaction with HLA-DR1. At the low affinity end of the maturation pathway, mutations in the hydrophobic ridge of the SEC3-wt template act to better fill the space between the molecular surface of this loop and the hydrophobic cleft that it fills on the HLA-DR1 α subunit molecular surface, corresponding to an increase, up to a threshold level, in the S_c value in this variant region of the interface. This provides an affinity improvement in the phage display mutant complexes to at least the intermediate level of the SEC3-3B1 variant. Then, when affinity gains from better shape complementarity are exhausted, augmentation of ΔASA_{apolar} improves the affinity of the complex further to the level of the high-affinity variant SEC3-3B2. In this system, the two biophysical factors, shape complementarity and buried hydrophobic surface area, each dominate one end of the affinity maturation pathway. Shape complementarity is increased initially, at which point expansion of the variant interface through additional hydrophobic surface can more effectively alter the affinity. Importantly, changes in ΔASA_{apolar} cannot explain early steps of affinity maturation, and changes in S_c values cannot explain later steps. In fact, the S_c value of the variant region is lower in the higher-affinity SEC3-3B2/HLA-DR1 complex than it is in the SEC3-3B1/HLA-DR1 complex. It is likely then that shape complementarity in this region of the interface has reached a threshold for the SEC3-3B1 and SEC3-3B2/HLA-DR1 complexes, above which it no longer affects binding affinity. Thus, one critical amino acid difference between SEC3-3B1 and SEC3-3B2, the mutation of Asn46 to Lys46, represents an instance in which shape complementarity can be sacrificed if retained above a critical threshold level, in order to gain energetically valuable buried hydrophobic surface area.

SEB Represents a Structural Intermediate on the SEC3 Affinity Maturation Pathway

SEB binds HLA-DR1 at the same site as does SEC3 (Jardetzky et al., 1994), with an affinity intermediate to that of SEC3-wt and SEC3-3B1 (Table 2). Outside of the hydrophobic ridge region, there are only very minor structural differences in the SEB/SEC3 interfaces formed with HLA-DR1, including two amino acid differences at positions 65 (Lys in SEB, Arg in SEC3) and 92 (Asn in SEB, Gln in SEC3). The components of the polar pocket that accepts HLA-DR1 Lysα39 are identical between these two SAGs, and accordingly, their structures are also highly similar (data not shown). Barring large energetic effects resulting from amino acid differences at SEB/SEC3 positions 65 and 92, HLA-DR1 binding affinity variability between SEB and SEC3 is likely due exclusively to differences in the relative sequences (Table 2) and structures of their hydrophobic ridge regions.

SEB displays a partly matured hydrophobic ridge when viewed within the context of the phage display mutagenesis affinity maturation process described here for SEC3. As in the case for SEC3 and its phage display variants, there appears to be no clear correlation between affinity for HLA-DR1 and the number or type of intermolecular contacts. The hydrogen bonds between the terminal atoms of Tyrα13 and Lysα67 and main chain SEB atoms are conserved as in all three SEC3/HLA-DR1 complexes. Also uncorrelated with the relative affinity of the SEB/HLA-DR1 complex are its hydrophobic ridge $\Delta ASA_{aggregate}$ and ΔASA_{polar} values (Table 2).

The SEB hydrophobic ridge exhibits those structural characteristics deemed important for SEC3/HLA-DR1 affinity maturation, namely augmentation of ΔASA_{apolar} and improvements in shape complementarity relative to SEC3-wt. As for other early mutagenesis events in the affinity maturation pathway of SEC3, $\Delta\Delta ASA_{apolar(SEB\text{-}SEC3)}$ cannot fully account for the relative affinity differences. Using our quantitative estimate of the hydrophobic effect of -21 cal mol^{-1} Å^{-2} (Sundberg et al., 2000) and the $\Delta\Delta ASA_{apolar(SEB\text{-}SEC3)}$ of 22 Å^2 (Table 2), we obtain a $\Delta\Delta G_{predicted(SEB\text{-}SEC3)}$ of -0.46 kcal mol^{-1}, significantly underestimating the actual $\Delta\Delta G_{b(SEB\text{-}SEC3)}$ of -0.96 kcal mol^{-1}. The S_c value for the interface formed by HLA-DR1 and the SEB hydrophobic ridge, at 0.758, is greater than for SEC3-wt but lower than for SEC3-3B1 and SEC3-3B2, and does not exceed the S_c value threshold observed in the SEC3 affinity maturation process. This data can be interpreted to mean that the increase in HLA-DR1 binding by SEB relative to SEC3-wt is due to both a more hydrophobic character of the ridge and better space filling of the cleft on the HLA-DR1 α subunit. SEB thus occupies an intermediate position on the SEC3 affinity maturation pathway at which point neither of the two biophysical factors dominates the maturation process. Accordingly, the directed evolution of the SEB/HLA-DR1 complex by mutagenesis of the SEB hydrophobic ridge would likely result in selective pressure to produce variants with reconstructed hydrophobic ridge regions that first attain the S_c value threshold level, and then maximize hydrophobic buried surface area.

Staphylococcus aureus produces a multitude of structurally related SAGs, including both SEC3 and SEB (Bohach et al., 1990; Dinges et al., 2000). Because SEB exhibits structural properties that allow its placement on the SEC3/HLA-DR1 affinity maturation pathway defined by SEC3-wt and the phage display variants SEC3-3B1 and SEC3-3B2, the directed evolution process reported in this study likely mimics at least one way in which the molecular evolution process is carried out by *S. aureus* in nature to produce SAGs with increased potency.

Functional Consequences of Affinity Matured SAG-MHC Interfaces

SAGs function through simultaneous interactions with class II MHC and T cell receptor (TCR) molecules resulting in the massive proliferation of T cells (Li et al., 1999; Sundberg et al., 2002). Superposition of X-ray crystal structures of the SEC3/14.3.d TCR β chain complex (Fields et al., 1996), the 2C $\alpha\beta$TCR (Garcia et al., 1996), and the SEC3/HLA-DR1 complex reported here

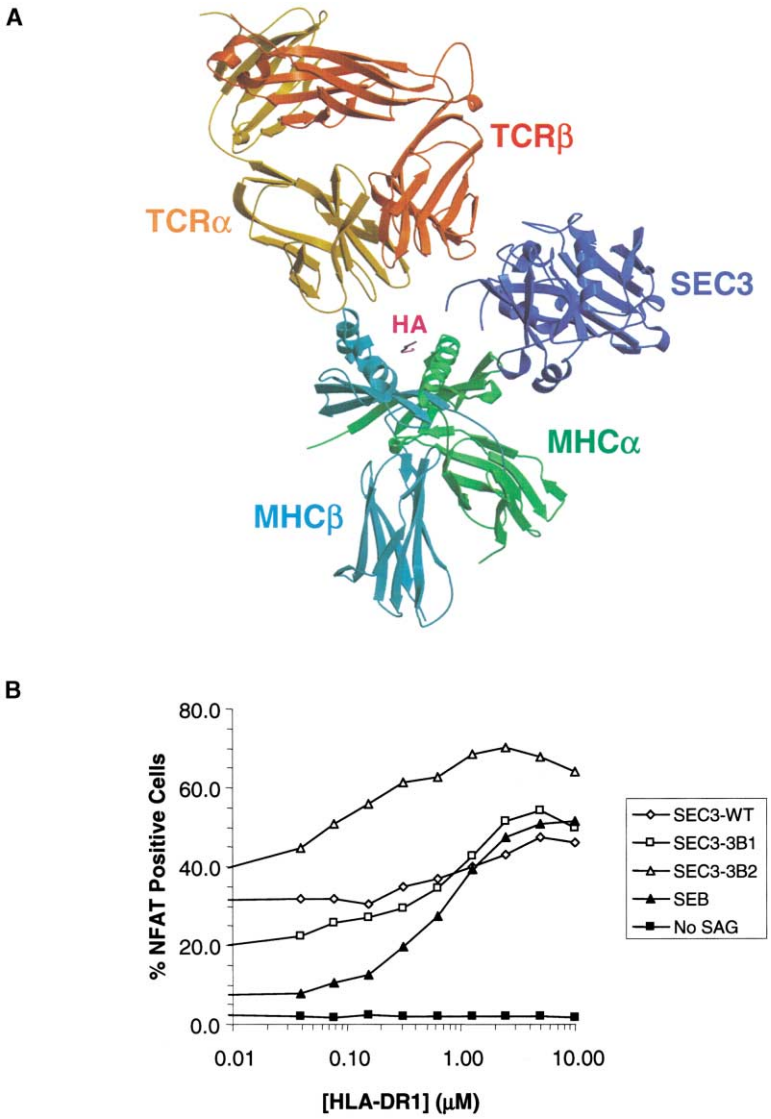

Figure 4. The Molecular Architecture of a Superantigen-Dependent T Cell Activation Complex and the Functional Consequences of Varied Affinity within Specific Protein-Protein Interfaces

(A) A molecular model of the SEC3-dependent MHC-SAG-TCR ternary complex composed of superposed portions of three X-ray crystal structures: the SEC3-wt/HLA-DR1 complex reported in this study, the SEC3/14.3.d TCR β chain complex (Fields et al., 1996), and the 2C αβTCR complex (Garcia et al., 1996). Colors are as follows: SEC3, blue; MHC α subunit, green; MHC β subunit, cyan; TCR α chain, orange; TCR β chain, red; hemagluttinin 306–318 peptide, magenta. Figure produced using Molscript (Kraulis, 1991) and Raster3D (Merritt and Bacon, 1997).

(B) NFAT activation in A5 T cell hybridomas which contain an NFAT-GFP expression cassette and express the 14.3.d TCR following 4.5 hr of stimulation by immobilized SEC3-wt (open diamonds), SEC3-3B1 (open squares), SEC3-3B2 (open triangles), SEB (closed triangles), or no SAG (closed squares) in the presence of various concentrations of soluble HLA-DR1.

results in a ternary T cell signaling complex in which SEC3 forms a wedge between the MHC and TCR molecules (Figure 4A). This supramolecular complex contains three distinct protein-protein interactions, including the SEC3/MHC α subunit, SEC3/TCR β chain, and MHC β subunit/TCR α chain interfaces. We have previously verified the direct MHC/TCR interaction in this complex biochemically (Andersen et al., 1999) and have quantified the cooperative energetic contributions it makes to the entire complex (Andersen et al., 2002). Superposition of X-ray crystal structures of the SEB/14.3.d TCR β chain complex (Li et al., 1998), the 2C αβTCR (Garcia et al., 1996), and the SEB/HLA-DR1 complex (Jardetzky et al., 1994) results in an SEB-dependent T cell signaling complex that is morphologically identical to the MHC/SEC3/TCR complex.

T cell activation by SEC3 and SEB is therefore regulated by the energetics of binding at these three protein-protein interfaces and their cooperative effects within the ternary complex. Although a direct correlation between ligand affinity and immunological potency of SAG-TCR interactions has been observed (Andersen et al., 2001b), affinity differences in the SAG-MHC interface appear to be more important for SAG-dependent T cell stimulation than affinity changes at the SAG-TCR binding site. SEC3 binds the 14.3.d TCR with nearly 50-fold higher affinity than does SEB [$K_{D(SEC3/14.3.d\ TCR)}$ = 3 μM (Leder et al., 1998); $K_{D(SEB/14.3.d\ TCR)}$ = 140 μM (Malchiodi et al., 1995)]. Conversely, SEC3 binds HLA-DR1 with approximately 5-fold lower affinity than does SEB [$K_{D(SEC3/HLA-DR1)}$ = 270 μM; $K_{D(SEB/HLA-DR1)}$ = 54 μM]. The concentration threshold for efficient T cell stimulation is 10-fold lower for SEB than for SEC3 (Leder et al., 1998), exactly the opposite expected if SAG interactions with MHC and TCR were of similar energetic importance in stabilizing the ternary complex.

To determine the consequences of the altered SAG-MHC molecular interfaces of SEC3-wt, SEC3-3B1, SEC3-3B2, and SEB in terms of biological activity, we assayed the T cell stimulatory properties of these SAGs

in the presence of varying concentrations of MHC molecules (Figure 4B). SEB, which is the least stimulatory in the absence of HLA-DR1, is most sensitive to the presence of soluble HLA-DR1 resulting in a nearly 10-fold increase in potency. SEC3-wt, SEC3-3B1, and SEC3-3B2 likewise exhibit enhanced potency as the concentration of HLA-DR1 increases, although their relative potency increases are not as large as for SEB. In addition, SEC3-3B1, SEC3-3B2, and SEB respond to HLA-DR1 at lower concentrations than does SEC3-wt, correlating with their higher affinities for HLA-DR1. In the absence of any SAG, no T cell stimulation is observed, regardless of soluble HLA-DR1 concentration.

Because the MHC and TCR molecules used in this assay are constant and all of the SAGs adopt an identical orientation within the supramolecular complex, the direct binding site between the MHC β subunit and the TCR α chain can be presumed irrelevant to the relative T cell stimulation profiles of the individual SAGs tested. Therefore, these stimulation profiles can be interpreted as the combinatory effects of the relative affinities of the SAG-MHC and SAG-TCR interfaces of the particular SAGs. Furthermore, SEC3-wt, SEC3-3B1, and SEC3-3B2 bind TCR with the same affinity (Andersen et al., 1999), and thus, their stimulation profiles should be dependent only on their relative affinities for HLA-DR1.

The peak stimulatory capacities of this panel of SAGs correlate with their relative affinities for HLA-DR1 (SEC3-wt $<$ SEB $<$ SEC3-3B1 $<$ SEC3-3B2). Thus, when HLA-DR1 concentration is not limiting, SAG-MHC affinities appear to dominate the T cell stimulation properties of these SAGs, in agreement with the results of more typical T cell stimulation assays (Leder et al., 1998). Presumably, the surface density of HLA-DR1 on APCs is relatively high, reflecting the point in our assay where HLA-DR1 concentration is no longer limiting. As HLA-DR1 concentrations become more limiting, though, SAG-TCR affinities play a more significant role in SAG-dependent stimulation. In the absence of HLA-DR1, T cell stimulation by SEC3-wt, SEC3-3B1, and SEC3-3B2, whose TCR affinities are equivalent, is primarily dependent on the immobilized SAG density. In the case of SEB, which has a nearly 50-fold lower affinity for the 14.3.d TCR β chain relative to SEC3 (Leder et al., 1998; Malchiodi et al., 1995), however, stimulation levels fall off dramatically with decreasing HLA-DR1 concentrations, and in the absence of HLA-DR1, SEB-dependent T cell stimulation is significantly lower than for SEC3-wt, SEC3-3B1, or SEC3-3B2, as is expected from its lower TCR affinity. T cell responses by SEC3-3B1, SEC3-3B2, and SEB at lower HLA-DR1 concentrations relative to SEC3-wt correspond to their higher HLA-DR1 affinities. Thus, affinity matured SAG-MHC interfaces can shift the energetic dominance of this binding site within the context of the biologically relevant MHC-SAG-TCR complex to lower MHC concentrations.

Experimental Procedures

Protein Production

HLA-DR1 was produced by in vitro refolding from *Escherichia coli* inclusion bodies in the presence of a molar excess of the influenza hemagglutinin peptide, residues 306–318 (Research Genetics), and purified according to published methods (Frayser et al., 1999). SEC3 residues 43–47 were randomized using degenerate oligonucleotides PCR, the resulting phage library selected by panning on immobilized HLA-DR1 molecules and SEC3-wt, SEC3-3B1, and SEC3-3B2 were isolated from *E. coli* periplasmic fractions as described previously (Andersen et al., 1999). SEB was cloned and produced in *S. aureus* strain RN 4220, as described (Bohach et al., 1990).

Crystallization and Data Collection

Crystals of HLA-DR1 complexed with SEC3-wt, SEC3-3B1, and SEC3-3B2 were grown at room temperature by hanging drop vapor diffusion by mixing 1 μl of complex solution (containing an equimolar ratio of SEC3 and HLA-DR1 at a total concentration of 10 mg/mL) with an equal volume of reservoir solution containing 0.1 M sodium acetate (pH 4.6), 10% ethylene glycol, and 2%–4% polyethylene glycol 4000. Crystals were transferred to cryoprotectant solution (mother liquor containing 25% ethylene glycol) just prior to mounting and flash cooling in the liquid nitrogen stream. X-ray diffraction data were from single crystals at 100 K at beamline ID-19 of the Structural Biology Center, Argonne National Laboratory for cocrystals of SEC3-wt/HLA-DR1 and SEC3-3B1/HLA-DR1, and at beamline X-12B of the National Synchrotron Light Source, Brookhaven National Laboratory for the SEC3-3B2/HLA-DR1 cocrystals. All SEC3/HLA-DR1 complexes crystallized isomorphously. Diffraction data were treated independently for all crystals and were processed and scaled using DENZO and SCALEPACK (Otwinowski and Minor, 1997). Data collection statistics are shown in Table 2.

Structure Determination and Refinement

The structures of the SEC3/HLA-DR1 complexes were each solved independently by molecular replacement methods using the program AMoRe (Navaza, 1994), with crystal structures of HLA-DR1 (PDB accession code 1SEB) and wild-type SEC3 (Deringer et al., 1996) as search models. The solution for HLA-DR1 was found first and its position fixed in order to locate SEC3. Refinement of each SEC3/HLA-DR1 complexes was also carried out independently using CNS (Brunger et al., 1998), including rigid-body refinement, iterative cycles of positional, torsion angle and temperature factor (*B*) refinement, interspersed with model rebuilding into σ_A-weighted $F_o - F_c$ and $2F_o - F_c$ electron density maps using XtalView (McRee, 1999). Water molecules were added only to $F_o - F_c$ density higher than 3σ and standard hydrogen-bonding geometry. The SEC3-3B2/HLA-DR1 structure was refined to an R_{cryst} value of 20.0% and an R_{free} value of 23.7% at 2.3 Å resolution. The SEC3-wt/HLA-DR1 and SEC3-3B1/HLA-DR1 structures were refined by an analogous process using a partially refined SEC3-3B2/HLA-DR1 structure as a starting model. R_{cryst} values of 19.2% and 19.5% and R_{free} values of 22.8% and 23.2% were obtained at 2.7 and 2.6 Å resolution for the SEC3-wt/HLA-DR1 and SEC3-3B1/HLA-DR1 structures, respectively. Refinement statistics for all of the complex structures are summarized in Table 2. Due to poor or nonexistent electron density, all three of the final models are missing residues 1–2 of the HLA-DR1 α chain, 108–110 of the HLA-DR1 β chain, and 99–105 of SEC3.

T Cell Stimulation

The potencies of SEC3-wt, SEC3-3B1, SEC3-3B2, and SEB T cell stimulation in the presence of MHC were assayed as described previously (Andersen et al., 2001a). In brief, Maxisorb microtiter plates (NUNC A/S Denmark) were coated overnight at 4°C with 50 μl each of SEC3-wt (0.3 μg/ml), SEC3-3B1 (0.6 μg/ml), SEC3-3B2 (0.3 μg/ml), or SEB (4 μg/ml) and subsequently blocked for 1 hr at room temperature using 2% bovine serum albumin in phosphate-buffered saline. The efficacy of coating was evaluated by ELISA. A 40 μM stock solution of HLA-DR1 was dialyzed against IMDM medium for 3 days at 4°C prior to serial dilution into SAG-coated wells in a final volume of 100 μl. A5 T cell hybridomas (1×10^5) expressing the 14.3.d $\alpha\beta$TCR (mouse Vβ8.2/Vα4.2) and containing an NFAT-GFP expression cassette (Bot et al., 1996) were added to each well in a volume of 50 μl. T cell stimulation was carried out over the course of 4.5 hr and NFAT activation measured by the presence of intracellular GFP. One hundred microliters medium was added to each well prior to detection of fluorescing cells by FACS.

Acknowledgments

We thank the staffs at beamline X-12B National Synchrotron Light Source, Brookhaven National Laboratory, and at beamline 19-ID Structural Biology Center, Argonne National Laboratory for assistance in data collection. This research was supported by NIH grants AI36900 and AI49564 (R.A.M.). E.J.S. is supported in part by a fellowship from the Arthritis Foundation.

Received: January 22, 2003
Revised: March 26, 2003
Accepted: May 27, 2003
Published: September 2, 2003

References

Andersen, P.S., Lavoie, P.M., Sekaly, R.P., Churchill, H., Kranz, D.M., Schlievert, P.M., Karjalainen, K., and Mariuzza, R.A. (1999). Role of the T cell receptor alpha chain in stabilizing TCR-superantigen-MHC class II complexes. Immunity *10*, 473–483.

Andersen, P.S., Geisler, C., Buus, S., Mariuzza, R.A., and Karjalainen, K. (2001a). Role of the T cell receptor ligand affinity in T cell activation by bacterial superantigens. J. Biol. Chem. *276*, 33452–33457.

Andersen, P.S., Menne, C., Mariuzza, R.A., Geisler, C., and Karjalainen, K. (2001b). A response calculus for immobilized T cell receptor ligands. J. Biol. Chem. *276*, 49125–49132.

Andersen, P.S., Schuck, P., Sundberg, E.J., Geisler, C., Karjalainen, K., and Mariuzza, R.A. (2002). Quantifying the energetics of cooperativity in a ternary protein complex. Biochemistry *41*, 5177–5184.

Bogan, A.A., and Thorn, K.S. (1998). Anatomy of hot spots in protein interfaces. J. Mol. Biol. *280*, 1–9.

Bohach, G.A., Fast, D.J., Nelson, R.D., and Schlievert, P.M. (1990). Staphylococcal and streptococcal pyrogenic toxins involved in toxic shock syndrome and related illnesses. Crit. Rev. Microbiol. *17*, 251–272.

Bot, A., Bot, S., Antohi, S., Karjalainen, K., and Bona, C. (1996). Kinetics of generation and persistence on membrane class II molecules of a viral peptide expressed on foreign and self proteins. J. Immunol. *157*, 3436–3442.

Brooijmans, N., Sharp, K.A., and Kuntz, I.D. (2002). Stability of macromolecular complexes. Proteins *48*, 645–653.

Brunger, A.T., Adams, P.D., Clore, G.M., DeLano, W.L., Gros, P., Grosse-Kunstleve, R.W., Jiang, J.S., Kuszewski, J., Nilges, M., Pannu, N.S., et al. (1998). Crystallography and NMR system: a new software suite for macromolecular structure determination. Acta Crystallogr. *D54*, 905–921.

CCP4 (Collaborative Computational Project 4) (1994). The CCP4 suite: programs for protein crystallography. Acta Crystallogr. D Biol. Crystallogr. *50*, 760–763.

Conte, L.L., Chothia, C., and Janin, J. (1999). The atomic structure of protein-protein recognition sites. J. Mol. Biol. *285*, 2177–2198.

DeLano, W.L. (2002). Unraveling hot spots in binding interfaces: progress and challenges. Curr. Opin. Struct. Biol. *12*, 14–20.

Deringer, J.R., Ely, R.J., Stauffacher, C.V., and Bohach, G.A. (1996). Subtype-specific interactions of type C staphylococcal enterotoxins with the T-cell receptor. Mol. Microbiol. *22*, 523–534.

Dinges, M.M., Orwin, P.M., and Schlievert, P.M. (2000). Exotoxins of Staphylococcus aureus. Clin. Microbiol. Rev. *13*, 16–34.

Dwyer, J.J., Dwyer, M.A., and Kossiakoff, A.A. (2001). High affinity RNase S-peptide variants obtained by phage display have a novel "hot-spot" of binding energy. Biochemistry *40*, 13491–13500.

Esnouf, R.M. (1997). An extensively modified version of MolScript that includes greatly enhanced coloring capabilities. J. Mol. Graph Model *15*, 132–134, 112–133.

Fields, B.A., Malchiodi, E.L., Li, H., Ysern, X., Stauffacher, C.V., Schlievert, P.M., Karjalainen, K., and Mariuzza, R.A. (1996). Crystal structure of a T-cell receptor beta-chain complexed with a superantigen. Nature *384*, 188–192.

Frayser, M., Sato, A.K., Xu, L., and Stern, L.J. (1999). Empty and peptide-loaded class II major histocompatibility complex proteins produced by expression in Escherichia coli and folding in vitro. Protein Expr. Purif. *15*, 105–114.

Garcia, K.C., Degano, M., Stanfield, R.L., Brunmark, A., Jackson, M.R., Peterson, P.A., Teyton, L., and Wilson, I.A. (1996). An alphabeta T cell receptor structure at 2.5 A and its orientation in the TCR-MHC complex. Science *274*, 209–219.

Hilser, V.J., Gomez, J., and Freire, E. (1996). The enthalpy change in protein folding and binding: refinement of parameters for structure-based calculations. Proteins *26*, 123–133.

Jardetzky, T.S., Brown, J.H., Gorga, J.C., Stern, L.J., Urban, R.G., Chi, Y.I., Stauffacher, C., Strominger, J.L., and Wiley, D.C. (1994). Three-dimensional structure of a human class II histocompatibility molecule complexed with superantigen. Nature *368*, 711–718.

Jones, S., and Thornton, J.M. (1996). Principles of protein-protein interactions. Proc. Natl. Acad. Sci. USA *93*, 13–20.

Kraulis, P.J. (1991). MOLSCRIPT: a program to produce both detailed and schematic plots of protein structures. J. Appl. Crystallogr. *24*, 946–950.

Kuntz, I.D., Chen, K., Sharp, K.A., and Kollman, P.A. (1999). The maximal affinity of ligands. Proc. Natl. Acad. Sci. USA *96*, 9997–10002.

Lavigne, P., Bagu, J.R., Boyko, R., Willard, L., Holmes, C.F., and Sykes, B.D. (2000). Structure-based thermodynamic analysis of the dissociation of protein phosphatase-1 catalytic subunit and microcystin-LR docked complexes. Protein Sci. *9*, 252–264.

Lawrence, M.C., and Colman, P.M. (1993). Shape complementarity at protein/protein interfaces. J. Mol. Biol. *234*, 946–950.

Leder, L., Llera, A., Lavoie, P.M., Lebedeva, M.I., Li, H., Sekaly, R.P., Bohach, G.A., Gahr, P.J., Schlievert, P.M., Karjalainen, K., et al. (1998). A mutational analysis of the binding of staphylococcal enterotoxins B and C3 to the T cell receptor beta chain and major histocompatibility complex class II. J. Exp. Med. *187*, 823–833.

Li, H., Llera, A., Tsuchiya, D., Leder, L., Ysern, X., Schlievert, P.M., Karjalainen, K., and Mariuzza, R.A. (1998). Three-dimensional structure of the complex between a T cell receptor beta chain and the superantigen staphylococcal enterotoxin B. Immunity *9*, 807–816.

Li, H., Llera, A., Malchiodi, E.L., and Mariuzza, R.A. (1999). The structural basis of T cell activation by superantigens. Annu. Rev. Immunol. *17*, 435–466.

Lowman, H.B. (1997). Bacteriophage display and discovery of peptide leads for drug development. Annu. Rev. Biophys. Biomol. Struct. *26*, 401–424.

Luque, I., and Freire, E. (2002). Structural parameterization of the binding enthalpy of small ligands. Proteins *49*, 181–190.

Ma, B., Wolfson, H.J., and Nussinov, R. (2001). Protein functional epitopes: hot spots, dynamics and combinatorial libraries. Curr. Opin. Struct. Biol. *11*, 364–369.

Malchiodi, E.L., Eisenstein, E., Fields, B.A., Ohlendorf, D.H., Schlievert, P.M., Karjalainen, K., and Mariuzza, R.A. (1995). Superantigen binding to a T cell receptor beta chain of known three-dimensional structure. J. Exp. Med. *182*, 1833–1845.

McRee, D.E. (1999). XtalView/Xfit–A versatile program for manipulating atomic coordinates and electron density. J. Struct. Biol. *125*, 156–165.

Merritt, E.A., and Bacon, D.J. (1997). Raster3D. Photorealistic Molecular Graphics. Methods Enzymol. *277*, 505–524.

Navaza, J. (1994). AMoRe: an automated package for molecular replacement. Acta Crystallogr. D Biol. Crystallogr. *50*, 157–163.

Nicholls, A., Sharp, K.A., and Honig, B. (1991). Protein folding and association: insights from the interfacial and thermodynamic properties of hydrocarbons. Proteins *11*, 281–296.

Otwinowski, Z., and Minor, W. (1997). Processing X-ray diffraction data collected in oscillation mode. Methods Enzymol. *276*, 307–326.

Sheinerman, F.B., Norel, R., and Honig, B. (2000). Electrostatic aspects of protein-protein interactions. Curr. Opin. Struct. Biol. *10*, 153–159.

Sundberg, E.J., and Mariuzza, R.A. (2000). Luxury accommodations:

the expanding role of structural plasticity in protein-protein interactions. Struct. Fold. Des. *8*, R137–R142.

Sundberg, E.J., and Mariuzza, R.A. (2002). Molecular recognition in antibody-antigen complexes. Adv. Protein Chem. *61*, 119–160.

Sundberg, E.J., Urrutia, M., Braden, B.C., Isern, J., Tsuchiya, D., Fields, B.A., Malchiodi, E.L., Tormo, J., Schwarz, F.P., and Mariuzza, R.A. (2000). Estimation of the hydrophobic effect in an antigen-antibody protein-protein interface. Biochemistry *39*, 15375–15387.

Sundberg, E.J., Li, Y., and Mariuzza, R.A. (2002). So many ways of getting in the way: diversity in the molecular architecture of superantigen-dependent T-cell signaling complexes. Curr. Opin. Immunol. *14*, 36–44.

Wodak, S.J., and Janin, J. (2002). Structural basis of macromolecular recognition. Adv. Protein Chem. *61*, 9–73.

Accession Numbers

The coordinates and structure factors for the SEC-wt/HLA-DR1, SEC3-3B1/HLA-DR1, and SEC3-3B2/HLA-DR1 complexes have been deposited in the Protein Data Bank with accession codes 1JWM, 1JWS, and 1JWU, respectively.